Hyper- and Viscoelastic Modeling of Needle and Brain Tissue Interaction

Craig A. Lehocky, Yixing Shi, and Cameron N. Riviere

Abstract— **Deep needle insertion into brain is important for both diagnostic and therapeutic clinical interventions. We have developed an automated system for robotically steering flexible needles within the brain to improve targeting accuracy. In this work, we have developed a finite element needle-tissue interaction model that allows for the investigation of safe parameters for needle steering. The tissue model implemented contains both hyperelastic and viscoelastic properties to simulate the instantaneous and time-dependent responses of brain tissue. Several needle models were developed with varying parameters to study the effects of the parameters on tissue stress, strain and strain rate during needle insertion and rotation. The parameters varied include needle radius, bevel angle, bevel tip fillet radius, insertion speed, and rotation speed. The results will guide the design of safe needle tips and control systems for intracerebral needle steering.**

I. Introduction

Soft tissue modeling of surgical procedures is inherent for both understanding tissue responses to instrumentation, as well as for guiding the design of the instrument itself. Particularly with regards to needle insertion into soft tissue, one of the most commonly performed medical procedures, much work has been done in regards to modeling how needles penetrate tissue as they traverse toward targets deep within the body [1], [2]. These procedures are commonly employed for brachytherapy [3], the delivery of radioactive seeds to deep locations in the body such as the prostate, and also to locally administer medications or perform biopsy. Deep needle and probe insertion is becoming more common in the awake human brain for biopsy [4], deep brain stimulation [5], and experimental therapies such as the direct delivery of therapeutics to tumors [6]. Especially in brain, tissue is both delicate and precious due to the limited nature of neuron regeneration.

Recently, technologies have been developed to advance flexible needles or probes to targets of interest deep within the body . This growing field of research offers to bypass the current limitations of rigid instrumentation, which rely on reaching the target along a linear path from the surface of the body or surface of the cerebral cortex. Flexible needles offer the potential to traverse from starting to target location, while avoiding obstacles along a traditionally straight path, such as the ventricles or neurovasculature. One such technology involves the use of robotically actuating thin, flexible needles with beveled-tips. When inserted, asymmetric tissue forces on the beveled-face cause the needle to curve in tissue. By rotating the base of the needle about its long axis, the direction of curvature can be altered, conferring steerability [7], [8]. Our group has developed a method to allow for the controllability of the amount of needle curvature by slowly spinning the needle in a duty-cycled manner during insertion [9], [10]. The command of both amount of curvature and directionality offers strong image-guided control. However, in the attempts to develop an efficacious technology, the effects of these flexible needles on brain tissue must be investigated.

The amount of curvature exhibited by flexible, bevel-tipped needles depends upon both tissue properties and needle parameters (material, diameter, bevel angle) [11]. While parameters that maximize the attainable curvature are optimal for steerability, the effects of the needle design and control parameters on brain tissue must be considered in order to develop a safe clinical prototype. Particularly in the case of duty-cycled needle steering, rotating the needle too quickly may result in coring or excessive shearing of tissue [12]. To study the effect of needle design and control parameters on brain tissue, we developed finite element method (FEM) models of the needle and tissue interaction during small insertions and rotations.

Obtaining accurate results from such models requires an accurate constitutive model of brain tissue. Miller and Chinzei [13] developed a nonlinear viscoelastic constitutive brain tissue model that replicated brain behavior at low strain rates consistent with neurosurgical procedures. Shortly thereafter, Miller [14] linearized the model to make the implementation of such a model possible in a FEM environment. The model consists of hyperelastic material properties that capture the instantaneous behavior of brain tissue, as well as viscoelastic properties that capture the time-dependent dynamic properties of the tissue. In this study, we developed a FEM implementation of the linearized hyperelastic viscoelastic brain tissue model. We created several bevel-tipped needle models with varying design parameters (radius, bevel angle, and bevel tip fillet radius). The various needle parameters are demonstrated in Fig. 1. Small insertions and rotations of the needle into the tissue were performed, and tissue levels of stress and strain were collected. These results will lead to the fabrication of the optimal needle tip for efficacy and safety in brain. Finally,

This work was supported in part by the U.S. National Institutes of Health (grant nos. R21EB012209 and T32EB003392).

C. A. Lehocky is with the Department of Biomedical Engineering, Carnegie Mellon University, Pittsburgh, PA 15213 (phone: 412-268-2023; fax: 412-268-7350; e-mail: calehocky@cmu.edu).

Y. Shi is with the Department of Biomedical Engineering, Carnegie Mellon University, Pittsburgh, PA 15213 (e-mail: yixings@andrew.cmu.edu).

C. N. Riviere is with the Robotics Institute and Department of Biomedical Engineering, Carnegie Mellon University, Pittsburgh, PA 15213(e-mail: camr@ri.cmu.edu).

978-1-4244-7929-0/14/$26.00 ©2014 IEEE

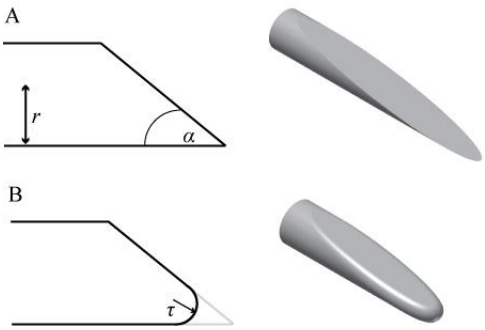

Figure 1. Illustration of the needle parameters varied in this study. A: bevel-tipped needle. B: bevel-tipped needle with fillet to decrease tissue damage. *r*: radius; α: bevel angle; *τ*: fillet radius.

the control inputs (rotational and insertion velocity) were varied while the strain rate of tissue monitored, in order to guide the actuation of the needle in actual tissue. The motivation of this study was to find the optimal needle design parameters and control inputs that will conform to brain safety levels and still confer steerability.

II. Methods

A. Brain Tissue Model

All simulations were developed and performed in Abaqus 6.12-1 (SIMULIA, Dassault Systèmes, Providence, RI, USA). The hyperelastic response was modeled with the Abaqus HYPERELASTIC command, with material constants C_{100} = 263 Pa and C_{200} = 491 Pa. The time-dependent tissue properties were implemented with the VISCOELASTIC command. For characteristic time t_1 = 0.5 s, g_1 = 0.450 and for characteristic time t_2 = 50 s, g_2 = 0.365 [14].

The tissue was modeled as a three-dimensional cube (Fig. 2). The size of the cube was increased during iterative testing to yield the dimensions of the tissue block at which stress, strain and strain rates converged, thus removing effects of boundary conditions interfering with needle-tissue interactions. The resulting dimensions for the cube were 12 mm lengths. On the center of the face coinciding with the long axis of the needle, a 3 x 3 mm square was partitioned and extended through the length of the tissue block in order to receive a mesh of higher density for the volume immediately surrounding the needle. Mesh density was varied in preliminary studies until results converged, leading to an outer tissue seed density of 2 mm and the inner tissue seed density of 0.4 mm. The tissue was meshed with 10-node quadratic tetrahedral elements with hybrid formulation (for tissue incompressibility) and constant pressure (C3D10H). Each tissue block was created such that the volume of the needle tip was removed from the tissue block, allowing the simulation to begin with the bevel-tip being completely immersed and in contact with tissue.

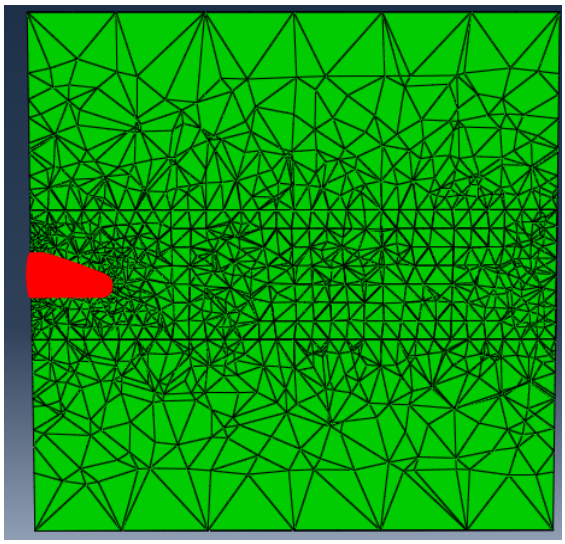
Figure 2. The geometry of the simulation, showing the 12-mm tissue cube in green, and a needle tip (radius 0.50 mm) in red.

Needle tips were modeled with varying parameters of radius, bevel angle, and bevel tip fillet radius. The various combinations of the twelve tested needle tips are listed in Table I. Not all permutations of radius, bevel angle and fillet radius were possible, due to geometrical and/or meshing constraints. The needle with r = 1.25 mm radius was designed with a perfectly rounded face (τ = 1.25 mm) to simulate a standard brain biopsy needle (2.5-mm Sedan Side-Cutting Biopsy Needle Kit, Elekta). The tips were developed with 0.1 mm of shaft behind the bevel face. Tips were seeded with high-density meshing to correspond to high-density meshing of the tissue block (0.4 mm seeds), and also meshed with C3D10H ten-node tetrahedral elements. Needle-tip material was simulated as linear elastic stainless steel (E = 200 GPa, ν = 0.29). A reference node was placed on the center of the circular (rear) surface of the needle, for specification of insertion and rotational velocities.

All sides of the tissue except for the face receiving the needle were constrained for all translational and rotational degrees of freedom to simulate the rigid conditions of the skull. At the beginning of simulation, the needle was situated within the negative space of the tissue. Contact procedures were applied through the general contact algorithm (Abaqus specification *all* with self*) and friction was applied to the needle-tissue interaction (μ = 0.5) [1].

TABLE I. Needle Design Parameters

Needle Radius (r) (mm)	**Bevel Angle (α)**	**Fillet radius (τ) (mm)**
0.32	10°	0.15
0.50	10° 20°	0.15 0.25
0.83	10° 20°	0.15 0.25 0.45
1.25	10°	1.25

Rotational and translational velocities were prescribed to the reference node on the center of the shaft of the needle. All needles were translated a total distance of 0.1 mm and rotated π/10 radians. For needle design parameter studies, simulations were performed with a translational velocity of 1 mm/s and rotational velocity of π rad/s for total simulation time of 0.1 s. For the control input rate study, three separate

rotational and translational velocity combinations were implemented for the 0.83 mm r 10° α 0.25 mm τ needle model: slow (0.5 mm/s and π/2 rad/s), medium (1 mm/s and π rad/s), and fast (2 mm/s and 2π rad/s).

Tissue safety data were compiled from *in vivo* studies that suggest critical damage to neurons and neurovasculature can occur above principal logarithmic strains of 0.19 [15] and strain rates above 10 s^{-1} [16]. We have adopted stress level thresholds from *in vivo* liver studies, conservatively setting the threshold at 120 kPa [17]. Stress, strain and strain rate values were recorded from the maximal element in the tissue mesh.

III. Results

A. Needle Design Parameters for Brain Safety

Figure 3 shows results of a typical simulation. Figure 4 displays the cumulative stress and logarithmic strain results for all twelve needle combinations listed in Table I. All needle simulations fell well within the allowable tolerance for stress in brain tissue (120 kPa). However, only a certain subset of the needles remained in allowable strain regions during insertion and rotation. No immediately discernable patterns for needle radius or bevel angle effects upon stress and strain are apparent; however, the largest contributing factor for stress and strain differences is the fillet radius, as seen in Fig. 5. Here, the 0.83 mm and 0.50 mm radius needles show decreasing maximal stress with increasing fillet radius. This trend also held true for strain (not shown). The roundness of the edges on the beveled-tip diminishes the localized high stress contact points within tissue that easily leads to tissue damage. This is most clear with to the relatively low values for stress and strain in Fig. 3 for the completely rounded biopsy needle (r = 1.25; green line).

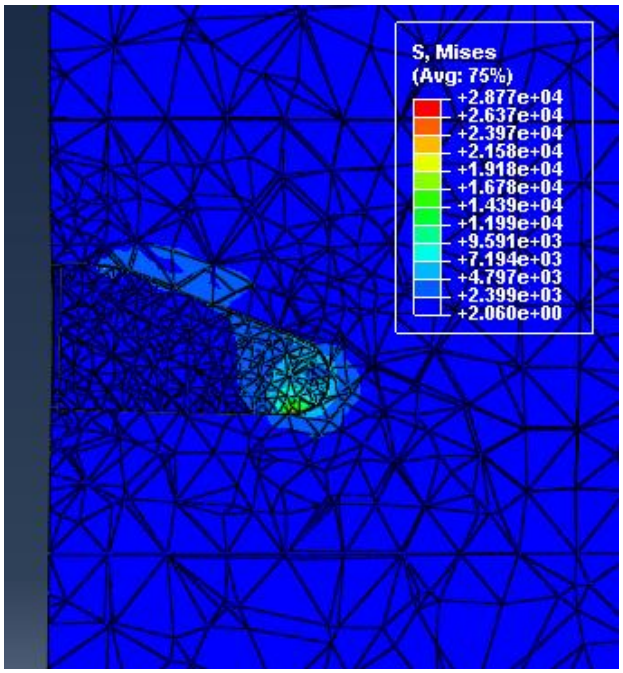

Figure 3. Final image of tissue stress response after insertion and rotation. The stress of the tissue is shown, with the 0.50 mm radius, 20° bevel angle, 0.25 mm fillet radius needle removed for clarity.

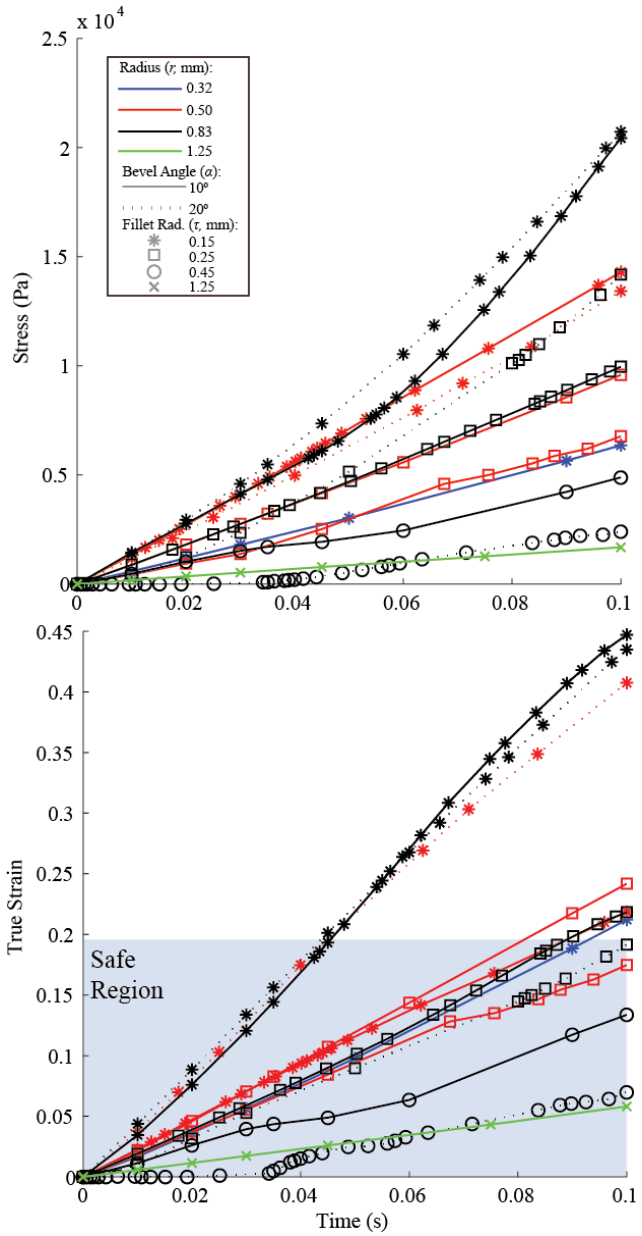

Figure 4. Stress and true strain for all needle combinations in Table I. All needles remained under established stress thresholds, but only certain combinations of needle parameters remained below the strain safety threshold for brain tissue.

B. Control Parameters for Strain Rate

A representative needle (0.83 mm radius, 10° bevel angle, 0.25 mm fillet radius) was implemented in three separate simulations to study the effect of velocity inputs on tissue strain rate. As discussed in the methods, the needle was inserted and rotated at three different combinations of velocities: "slow," "medium," and "fast," while tissue strain rates were recorded. Fig. 6 displays the results for the rate study. There is a clear indication that, as expected, strain rates increase with increasing combinations of insertion and rotational velocity. The effects of the viscoelastic tissue properties can be observed in the "slow" condition, where unlike the two faster conditions, the tissue has sufficient time

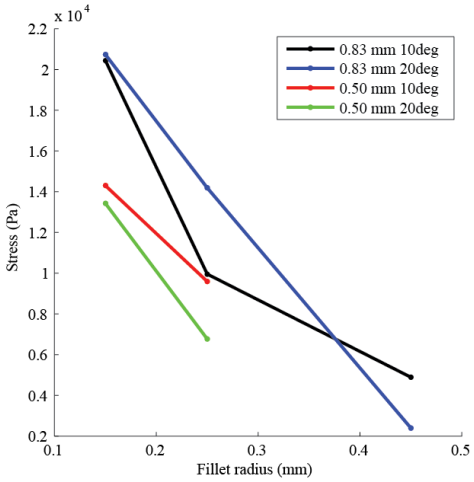

Figure 5. Maximum stress as a function of fillet radius for several needles. Stress decreases with increasing fillet radius across needle radius and bevel angle (as does strain (not shown)).

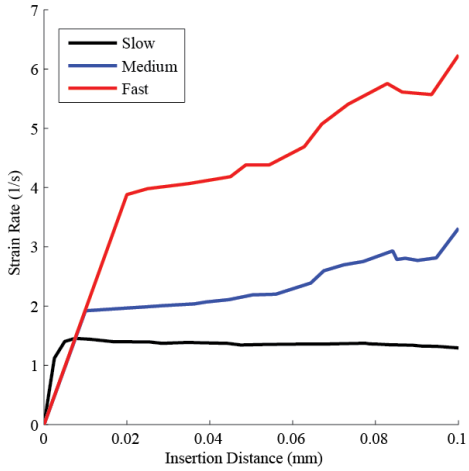

Figure 6. Tissue strain rates as a function of slow (0.5 mm/s and $\pi/2$ rad/s), medium (1 mm/s and π rad/s), and fast (2 mm/s and 2π rad/s) needle insertion and rotation. These results were obtained using a needle with 0.83 mm radius, 10° bevel angle, 0.25 mm fillet radius.

to relax during insertion and the strain rate does not continually increase during needle steering. All conditions satisfy the strain rate threshold for safety in the brain.

IV. Discussion

The linear hyperelastic, viscoelastic FEM model of brain tissue demonstrated that the fillet radius of needles, decreasing the effective sharpness of the needle, has a large effect on tissue safety. The trade-off for having larger fillet radii is that there is a decrease in surface area of the bevel face, which is necessary for achieving curvature in tissue. Thus, choosing a needle design that has the smallest allowable fillet radius is optimal for maximal steerability and sufficient safety.

The study of insertion and rotation speeds shows that inserting and rotating at slow speeds allows tissue time to relax, reducing strain rates. The set of results presented in Fig. 6 is only a small beginning, of course. Tests over a much greater range of insertion and rotation speeds and displacements are needed in order to allow selection of an optimum performance envelope for safe needle steering in the brain.

References

[1] M. Oldfield, D. Dini, G. Giordano, and F. Rodriguez Y Baena, "Detailed finite element modelling of deep needle insertions into a soft tissue phantom using a cohesive approach," *Comput. Methods Biomech. Biomed. Eng.*, vol. 16, no. 5, pp. 530–543, Jan. 2013.

[2] H. W. Nienhuys and A. F. van der Stappen, "A computational technique for interactive needle insertions in 3D nonlinear material," in *Proc. IEEE Int. Conf. Robot. Autom.*, 2004, vol. 2, pp. 2061–2067.

[3] O. Goksel, S. E. Salcudean, and S. P. DiMaio, "3D simulation of needle-tissue interaction with application to prostate brachytherapy," *Comput. Aided Surg.*, vol. 11, no. 6, pp. 279–288, 2006.

[4] F. Chan, I. Kassim, C. Lo, C. L. Ho, D. Low, B. T. Ang, and I. Ng, "Image-guided robotic neurosurgery--an in vitro and in vivo point accuracy evaluation experimental study," *Surg. Neurol.*, vol. 71, no. 6, pp. 640–7, 2009.

[5] L. Niu, L. Y. Ji, J. M. Li, D. S. Zhao, G. Huang, W. P. Liu, Y. Qu, L. T. Ma, and X. T. Ji, "Effect of bilateral deep brain stimulation of the subthalamic nucleus on freezing of gait in Parkinson's disease," *J. Int. Med. Res.*, vol. 40, no. 3, pp. 1108–1113, 2012.

[6] S. Kunwar, M. D. Prados, S. M. Chang, M. S. Berger, F. F. Lang, J. M. Piepmeier, J. H. Sampson, Z. Ram, P. H. Gutin, R. D. Gibbons, K. D. Aldape, D. J. Croteau, J. W. Sherman, and R. K. Puri, "Direct intracerebral delivery of cintredekin besudotox (IL13-PE38QQR) in recurrent malignant glioma: a report by the Cintredekin Besudotox Intraparenchymal Study Group," *J. Clin. Oncol.*, vol. 25, no. 7, pp. 837–844, 2007.

[7] R. J. Webster III, J. Memisevic, and A. M. Okamura, "Design considerations for robotic needle steering," in *Proc. IEEE Int. Conf. Robot. Autom.*, 2005, pp. 3599–3605.

[8] R. J. Webster III, J. S. Kim, N. J. Cowan, G. S. Chirikjian, and A. M. Okamura, "Nonholonomic modeling of needle steering," *Int. J. Robot. Res.*, vol. 25, no. 5–6, pp. 509–525, 2006.

[9] J. A. Engh, G. Podnar, S. Y. Khoo, and C. N. Riviere, "Flexible needle steering system for percutaneous access to deep zones of the brain," in *Proc. 32nd IEEE Northeast Bioeng. Conf.*, 2006, pp. 103–104.

[10] D. Minhas, J. Engh, M. Fenske, and C. Riviere, "Modeling of needle steering via duty-cycled spinning," in *Proc. Annu. Int. Conf. IEEE Eng. Med. Biol. Soc.*, 2007, pp. 2756–9.

[11] S. Misra, K. B. Reed, B. W. Schafer, K. T. Ramesh, and A. M. Okamura, "Mechanics of flexible needles robotically steered through soft tissue," *Int. J. Robot. Res.*, vol. 29, no. 13, pp. 1640–1660, 2010.

[12] M. A. Meltsner, N. J. Ferrier, and B. R. Thomadsen, "Observations on rotating needle insertions using a brachytherapy robot," *Phys. Med. Biol.*, vol. 52, pp. 6027–6037, 2007.

[13] K. Miller and K. Chinzei, "Constitutive modelling of brain tissue: Experiment and theory," *J. Biomech.*, vol. 30, no. 11–12, pp. 1115–1121, 1997.

[14] K. Miller, "Constitutive model of brain tissue suitable for finite element analysis of surgical procedures," *J. Biomech.*, vol. 32, pp. 531–537, 1999.

[15] D. I. Shreiber, A. C. Bain, and D. F. Meaney, "In vivo thresholds for mechanical injury to the blood-brain barrier," in *Proc. 41st Stapp Car Crash Conference*, 1997, pp. 277–291.

[16] B. Morrison III, H. L. Cater, C. C.-B. Wang, F. C. Thomas, C. T. Hung, G. A. Ateshian, and L. E. Sundstrom, "A tissue level tolerance criterion for living brain developed with an in vitro model of traumatic mechanical loading," *Stapp Car Crash J.*, vol. 47, pp. 93–105, 2003.

[17] S. De, J. Rosen, A. Dagan, B. Hannaford, P. Swanson, and M. Sinanan, "Assessment of tissue damage due to mechanical stresses," *Int. J. Rob. Res.*, vol. 26, no. 11–12, pp. 1159–1171, 2007.